Building and Environment 290 (2026) 114116

Contents lists available at ScienceDirect

Building and Environment

journal homepage: www.elsevier.com/locate/buildenv

Indoor Environmental and Energy Performance Analysis of Horizontal BIPV Windows and Their Potential to Meet South Korean ZEB Standards

A Young Kim [a], Bo Rang Park [a], Yong Gi Jung [a], Sang Hun Yeon [b], Yongseok Jun [c], Jin Woo Moon [a,*]

[a] School of Architecture and Building Science, Chung-Ang University, 84, Heukseok-ro, Dongjak-gu, Seoul, 06974, South Korea
[b] Department of Architecture, College of Engineering, Korea University, Anam-ro, Seongbuk-gu, 145, Seoul, 02841, South Korea
[c] Department of Integrative Energy Engineering, Graduate School of Energy and Environment, College of Engineering, Korea University, Anam-ro, Seongbuk-gu, 145, Seoul, 02841, South Korea

ARTICLE INFO

Keywords:
Window type-building integrated photovoltaic
Zero energy building (ZEB)
Single-crystal silicon (C-SI)
Thermo-optical property
Energy self-sufficiency ratio (ESSR)

ABSTRACT

The building sector accounts for about 38 % of global carbon emissions, making the realization of zero-energy buildings (ZEBs) a key step toward carbon neutrality. This requires improvements in building energy efficiency and the integration of renewable energy sources. This study evaluates the indoor environmental and energy performance of a horizontal solar cell-integrated window (HSC_W), a novel window-type BIPV system, to assess its suitability as a building envelope component and optimize its visible light transmission (VLT) and solar heat gain coefficient (SHGC). Mock-up experiments and computer simulations were conducted for Low-e windows and HSC_W to analyze indoor environmental performance, photovoltaic (PV) generation, and building energy consumption, while optimizing VLT–SHGC combinations. Mock-up results showed that HSC_W reduced indoor illuminance relative to Low-e windows but improved the thermal environment by blocking solar radiation. Simulations indicated that HSC_W increased lighting energy consumption by 6.0 % and heating by 9.5 % compared to Low-e windows, but reduced cooling by 14.6 %, leading to a net 1.3 % decrease in total energy use. Annual PV generation of 12,066.2 kWh further reduced net energy consumption by 21.1 %. Additional optimization of thermo-optical properties achieved another 2.27 % reduction under optimal conditions (VLT: 60 %, SHGC: 0.4). Based on the ZEB Grade 5 feasibility scale in the Republic of Korea, the energy self-sufficiency ratio (ESSR) of HSC_W varied with VLT–SHGC combinations, with four of nine exceeding 20 %, thus meeting mandatory ZEB requirements. These results provide a foundation for advancing HSC_W as an energy-efficient envelope component and expanding its applications.

Abbreviations

BIPV	Building-integrated photovoltaic
PV	Photovoltaic
c-Si	Single-crystal silicon
NDC	Nationally determined contribution
LEDS	Long-term Low Greenhouse Gas Emission Development Strategies
ZEB	Zero-energy building
VLT	Visible light transmission (%)
SHGC	Solar heat gain coefficient
DHW	Domestic hot water
DF	Daylighting factor (%)
FAWL	Floor area within limits
UR	Uniformity ratio
IAM	Incidence angle modifier
ESSR	Energy self-sufficiency ratio (%)
WWR	Window-to-wall ratio (%)
STC	Standard test condition
ASHRAE	American Society of Heating, Refrigerating and Air-Conditioning Engineers
AHU	Air handling unit
EHP	Electric heat pump
EUI	Energy use index (kWh/m^2)
IQR	Interquartile range
LEED	Leadership in Energy and Environmental Design
BREEAM	Building Research Establishment Environmental Assessment Method
G-SEED	Green Standard for Energy and Environmental Design

* Corresponding author.
E-mail address: gilerbert73@cau.ac.kr (J.W. Moon).

https://doi.org/10.1016/j.buildenv.2025.114116
Received 1 October 2025; Received in revised form 24 November 2025; Accepted 8 December 2025
Available online 9 December 2025
0360-1323/© 2025 Elsevier Ltd. All rights are reserved, including those for text and data mining, AI training, and similar technologies.

1. Introduction

According to a report by the International Energy Agency (IEA), global CO_2 emissions reached a record high of approximately 36.8 gigatons in 2021, with buildings responsible for about 38 % of the total [1]. Because the building sector represents a major source of global carbon emissions, there is an urgent need to reduce greenhouse gas emissions and achieve carbon neutrality in buildings. In particular, improving energy efficiency and reducing carbon emissions during the operational phase of buildings have been emphasized as essential measures for building decarbonization [2].

In response to this call, many countries have introduced carbon-neutral development policies for industry, transport, and buildings. For example, the European Union, through the European Green Deal, is pursuing mandatory Nearly Zero Energy Building (NZEB) standards for all new buildings by 2030 [3] while, in the United States, the Inflation Reduction Act has introduced large-scale investment in and incentives for the decarbonization of buildings [4]. Japan is expanding the deployment of zero-energy homes (ZEH) and zero-energy buildings (ZEB), while China is promoting zero-energy buildings and strengthening green building certification [5,6]. In line with these trends, the Korean government declared a 2050 carbon-neutral target in 2020, submitted its 2030 Nationally Determined Contribution (NDC) and 2050 Long-term Low Greenhouse Gas Emission Development Strategies (LEDS) framework to the UN, and enacted the Framework Act on Carbon Neutrality in 2021 to institutionalize its policy vision and governance [7,8].

For the building sector to achieve carbon neutrality, energy consumption should be minimized and the remaining energy demand should be met through renewables that do not emit greenhouse gases. To achieve this, the Republic of Korea's ZEB certification system, implemented in 2023, is currently being expanded in phases depending on the building size and type. The ZEB certification system categorizes buildings into six grades (+ to 5) based on their energy self-sufficiency ratio (ESSR), which is defined as the ratio of renewable energy produced by the building to its annual primary energy consumption: Grade + (≥120 %), Grade 1 (≥100 %), Grade 2 (≥80 %), Grade 3 (≥60 %), Grade 4 (≥40 %), and Grade 5 (≥20 %). Starting in 2025, public buildings with a gross floor area above 500 m^2 and private buildings with a floor area larger than 1,000 m^2 will be required to achieve at least ZEB Grade 5 [9]. The government aims to gradually expand these mandatory requirements, ultimately targeting ZEB status for all buildings. The ESSR calculations follow official Korean building energy-efficiency guidelines and ZEB certification standards, dividing annual renewable energy production by annual primary energy consumption. Within this framework, the application of building-integrated renewable energy technologies, such as window-type building-integrated photovoltaic (BIPV) systems, has been emphasized as a key measure for ZEB implementation [10]. The use of renewable energy is also important for achieving carbon neutrality and the NDC. In Korea, the proportion of renewable energy photovoltaic (PV) generation has increased from 3.5 % in 2013 to 10.1 % in 2024, with solar power accounting for 45.0 % of the total, recording the highest proportion [11]. However, because many solar PV generation systems are currently installed in locations with limited space such as roofs, the pursuit of ZEBs has structural limitations. In this context, BIPV systems are a key technology for improving energy self-sufficiency. Unlike conventional solar systems, the deployment of BIPV systems requires consideration of the role of the building exterior material, PV generation, and the aesthetics of the building. Currently, some BIPV products are being commercialized, including specialized modules for building-specific applications, exterior cladding materials, and colored products [12].

Recent approaches to the development of BIPVs have shifted from simply attaching generic PV modules to existing building components to integrating specially designed modules consisting of building envelope materials, such as insulation and glazing. Public, commercial, and educational buildings that are characterized by a high window-to-wall ratio (WWR) are particularly well-suited for the installation of window-type BIPV systems. Semi-transparent PV elements can outperform opaque alternatives by directly replacing conventional glazing while using established curtain wall installation techniques, thus improving constructability and enabling active on-site energy generation via the building facade [13,14].

The PV cells used in BIPVs generally have a lower conversion efficiency at higher cell temperatures. To mitigate this, modules often adopt darker tints with lower visible light transmission (VLT), which can degrade aesthetics and outward visibility [15]. Alternative transparent or semi-transparent technologies such as dye-sensitized solar cells (DSSCs), cadmium telluride (CdTe), copper indium gallium selenide (CIGS), and perovskite cells are under development, yet they still lack sufficient long-term efficiency and durability for building applications. While numerous studies have aimed to overcome the limitations of existing window solutions [16–22], important gaps remain, including comprehensive, quantitative assessments of how the thermo-optical properties of BIPV windows affect indoor daylighting, thermal conditions, and whole-building energy use [23–25]. Prior research has primarily focused on PV efficiency, with few studies providing a holistic evaluation of window-type BIPV systems as glazing components that must simultaneously satisfy daylighting, thermal, and energy requirements [26–32]. Robust evaluation frameworks that combine mock-up experiments with building energy simulations are also needed to improve the commercial prospects of these systems.

Accordingly, this study conducts an integrated assessment of a horizontal solar cell-integrated window (HSC_W) system, focusing on its practical feasibility for use in buildings and its potential contribution to Korea's ZEB obligations. We compare its indoor environmental performance (i.e., indoor air temperature, illuminance, and the front and rear glass temperatures) and PV generation against Low-e glazing using mock-up experiments and quantify overall energy use and PV generation using simulations. We also parametrize the thermo-optical properties of the HSC_Ws to identify optimal combinations and evaluate their ability to meet ZEB Grade 5 standards by calculating the ESSR for nine designs. This research thus seeks to evaluate the ability of the proposed HSC_W system to improve building energy performance while enhancing energy self-sufficiency and to inform the design and deployment of window-type BIPV systems within Korea's ZEB policy framework.

2. Structural characteristics and design principles of the HSC_W system

In window-type BIPV systems, the most important parameters are the VLT and PV efficiency. Transparent PVs typically limit visible absorption to increase their transparency, which reduces their PV efficiency; consequently, high-efficiency single-crystal silicon (c-Si) cells have typically been used in fixed rooftop arrays or opaque shading devices rather than in windows. Nevertheless, c-Si solar cells possess several advantages, including high photoelectric conversion efficiency, excellent durability, and stability, suggesting that their application in windows could potentially overcome the limitations of existing solar cell technologies [33–37].

The HSC_Ws consisted of PV cells as the generating element and inter-cell gaps aligned horizontally that admitted daylight. The PV cells were c-Si with a rated output of 121.7 W under STC; detailed specifications are presented in Table 1. Fig. 1 presents a cross-sectional diagram and corresponding layer photographs of the HSC_W system. The exterior HSC array was fabricated by cutting monocrystalline silicon solar cells into 166 mm × 10 mm segments and connecting four segments in a single row to form a slit-shaped strip. This strip was then arranged horizontally, parallel to the occupant's line of sight, creating a blind-like configuration. The gaps between adjacent cells were filled with transparent PDMS, which was used to protect the cells from external environmental exposure, maintain their structural alignment,

Table 1
Electrical performance specifications for the PV cells used in the proposed HSC_W system.

Type	Data
Cell type	Crystalline silicon solar cell (c-Si)
PV module area (m^2)	0.792
PV efficiency (%)	22.6
P_{max} (W)	121.7
I_{sc} (A)	6.9
V_{oc} (V)	24.3
I_{mp} (A)	6.3
V_{mp} (V)	19.4

and ensure that the window was airtight. The central layer incorporated a 13mm argon-filled cavity to enhance air tightness and thermal resistance, while the interior-side Low-e glazing reduced the radiative heat transfer and improved the overall energy performance. The mock-up window employed in this study thus contained a three-layered IGU system consisting of HSC (22 mm), argon (13 mm), and Low-e glazing (6 mm).

Due to this structural configuration, incident solar radiation reached the cell surface at a favorable angle, thereby improving the PV conversion efficiency, while the horizontal slits allowed both outward visibility and VLT to be maintained indoors. Unlike conventional opaque BIPV modules composed of front glass and a rear backsheet, where power generation is limited to single-side irradiation and installation flexibility is restricted, the HSC_W system adopted an open, non-opaque, dual-sided configuration, offering greater suitability for various building envelope conditions. Although the prototype tested in the present study employed c-Si, the architecture can be adapted to other highly efficient cell technologies, supporting its wider adoption. Accordingly, the proposed HSC_W system is a promising candidate for use in ZEBs.

3. Experimental and simulation methodology

In this study, to verify the applicability of the HSC_W system as a component of the building envelope, we conducted mock-up experiments in parallel with computer simulations. We first constructed a mock-up experiment environment to measure the indoor environmental performance and PV generation of the proposed system. We then conducted computer simulations to quantitatively evaluate the building energy performance when the HSC_W system is employed.

3.1. Mock-up environment and monitoring system

The mock-up environment was installed on the rooftop of a university building in Seoul, Korea (37.5 °N, 127.0 °E). As shown in Fig. 2(a), the mock-up was oriented due south and elevated 2,400 mm above the roof deck to minimize shading and solar obstruction from the surrounding structures. The mock-up dimensions were 1,410 mm (H) × 1,030 mm (W) × 1,030 mm (D). The building envelope was constructed with EPS panels with a thermal transmittance of 0.240 W/m^2·K. A window was installed on the front side, and ventilation openings measuring 30 mm × 30 mm were placed on the right and rear sides to prevent heat accumulation and overheating inside the test cell (Fig. 2(b)). Both an HSC_W and a Low-e window were tested, with the latter serving as a control for performance comparison. The tested windows measured 720 mm × 1,100 mm and included double glazing. The windows met Korean energy-saving design standards in terms of thermal transmittance for the Central Region 2 climate zone [38].

This mock-up installation was designed to systematically verify thermal and optical performance under single-variable conditions that are difficult to isolate in real buildings, while collecting data for the indoor air temperature, indoor illuminance, front and rear glass surface temperatures, and PV generation. The data were used to analyze the environmental and energy performance of the HSC_W system as a building envelope component and as a potential reference for the planning, operation, and maintenance of future HSC_W demonstrations.

Real-time monitoring was used to track changes in HSC_W PV performance, check for errors, and capture variation in the weather. The mock-up experiment ran for approximately three months from October 1, 2024, to December 31, 2024, during which data for 17 variables were

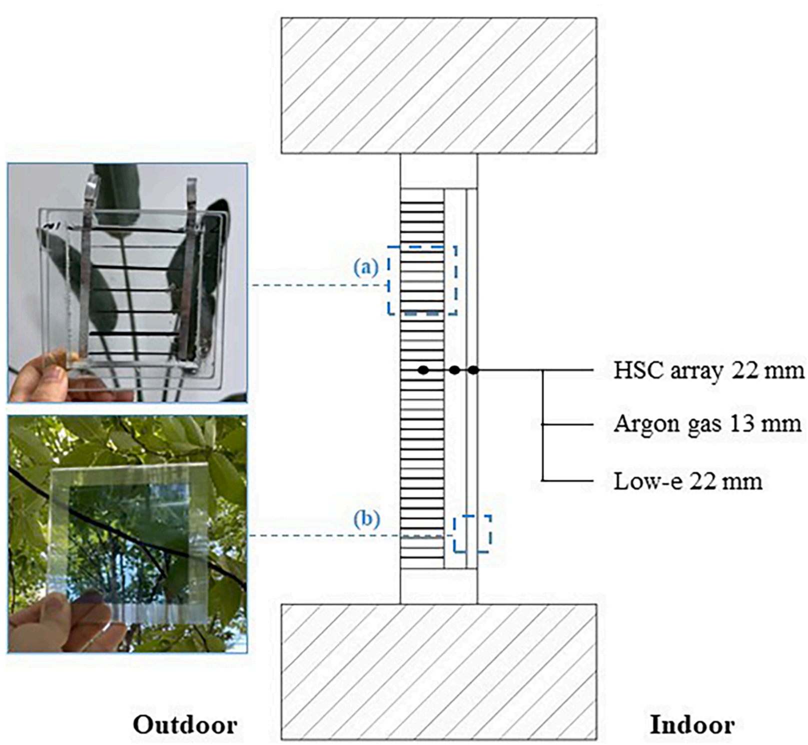

Fig. 1. Structural characteristics of the (a) exterior and (b) interior sides of the proposed HSC_W system.

(a) Photograph of the mock-up installation.

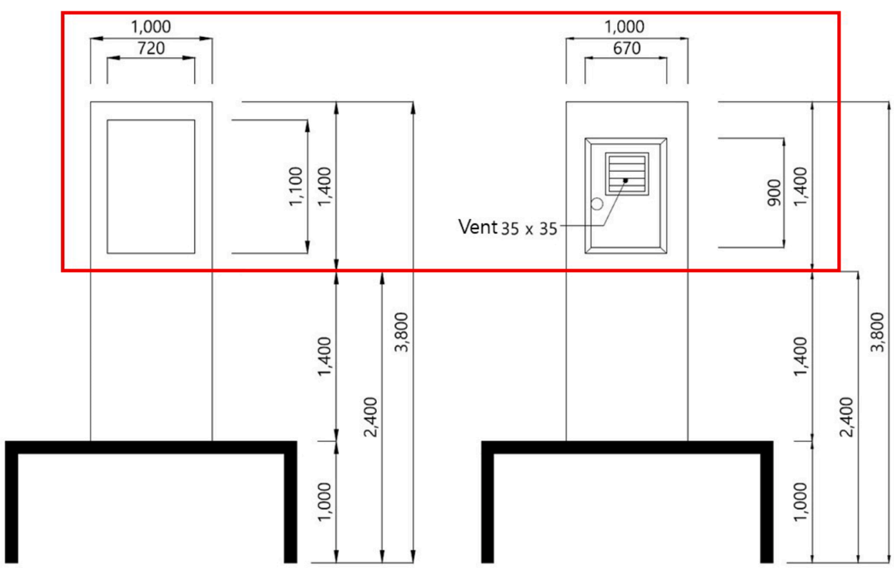

(b) Front and rear views of the mock-up.

Fig. 2. Mock-up experimental setup.

collected at 5 min intervals. The collected data were grouped into indoor environmental variables, weather data, and electrical characteristics. The monitoring system configuration is presented in Fig. 3.

Each sensor was connected by channel to enable measurement. Because no inverter was installed in the test environment, only DC electrical data were collected. For PV performance analysis, an I-V tester with maximum power point tracking (MPPT) was used to construct I-V curves under varying irradiance, temperature, and load conditions. Environmental sensors measured the temperature of the front and rear glass surfaces and the indoor air of the mock-up. Signals were digitized using a data acquisition (DAQ) system and stored on a server. The irradiance sensor met ISO 9060 class 2 requirements for the precise measurement of solar radiation incident on horizontal and tilted planes [39]. All of the equipment was connected with a data logger for real-time monitoring. The DAQ system, server PC, and electronic load were housed in a dedicated enclosure to protect the equipment from outdoor conditions and to minimize thermal effects, with a controller included to monitor the overall system and control each device. Measured data were stored and managed remotely via software installed on the monitoring server. A real-time dashboard was employed to visualize the indoor illuminance, front and rear glass temperatures, indoor air temperature, and PV generation for time-series analysis. All data were saved to the server in CSV format and could be accessed remotely from external PCs via a TCP/IP-based protocol.

3.2. Computer simulation software and target building settings

For building energy performance and PV generation analysis, we used DesignBuilder (ver. 7.0.2.003) in combination with EnergyPlus (ver. 9.2.0). DesignBuilder is a dynamic energy simulation tool based on EnergyPlus that allows detailed analysis of hourly building energy consumption [40]. This program supports settings for activity, construction, openings, lighting, and HVAC, among others, and these inputs are aligned with major international standards such as LEED, EN ISO

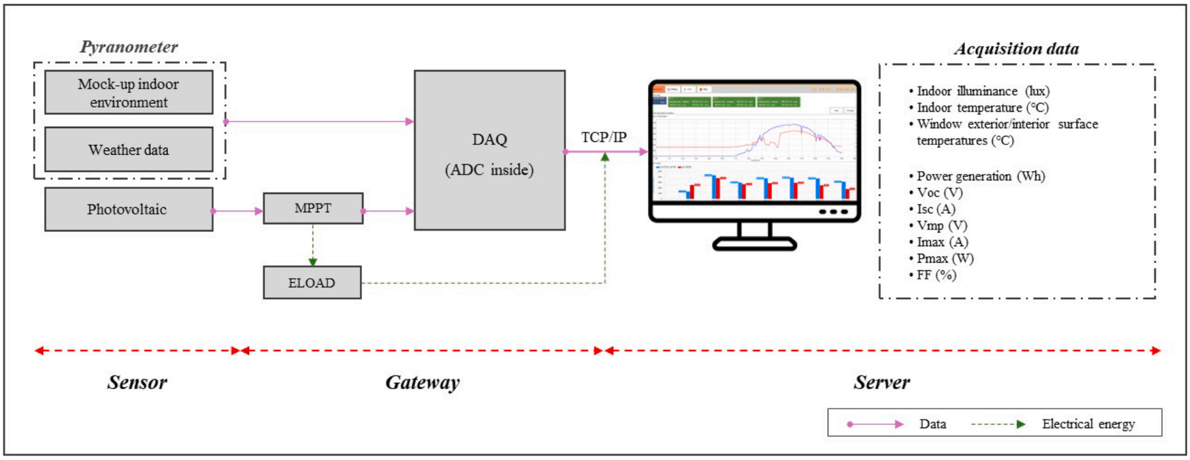

Fig. 3. Monitoring system configuration for the mock-up environment.

13790, and ASHRAE 90.1 [41,42]. The reliability of DesignBuilder and EnergyPlus for the evaluation of thermal and energy performance has been demonstrated in numerous prior studies [43–46]. In the present study, we used DesignBuilder for 3D modeling and whole-building energy analysis, while EnergyPlus was employed concurrently to evaluate power generation by individual PV panels and shading effects.

The target building was set as a typical medium-sized public office building with a gross floor area of approximately 2,202.2 m^2 across seven stories (Fig. 4). With a gross floor area of ≥1,000 m^2, this building was in accordance with Korea's ZEB obligation threshold. The building was oriented south, with an aspect ratio of approximately 1.5:1 [47]. Each floor contained six office spaces (5.5 m × 6.4 m), and each space had a window installed measuring 4.32 m in width and 2.20 m in height.

The thermal performance of the building envelope followed the legal U-value requirements for the Central Region 2 climate zone (Seoul). The heating and cooling source was an individual electric heat pump (EHP) system typical of medium-sized offices. Setpoint temperatures and operating periods were assigned to reflect local climate conditions. Office equipment loads were set using statistical data representative of medium-sized office buildings [48]. The indoor illuminance followed office-use lighting levels, and a dimming control strategy was employed to assess the impact of the window type on lighting energy [49]. Following prior studies, we adopted the "Linear off" method within DesignBuilder, which has been identified as one of the most effective embedded control modes [50]. Detailed information on the target building is presented in Table 2.

Seoul, Korea, is classified as climate zone 4A (mixed-humid) under ASHRAE categorization and is located at approximately 37.56 °N, 127.98 °E. The monthly average maximum and minimum temperatures are about 17.9°C and 10.2°C, respectively, indicating a temperate climate. The annual heating degree days (base 18°C) range from 2,600 to 2,800°C·day, whereas the cooling degree days (base 18°C) range from 1,200 to 1,400°C·day, indicating a heating demand that is approximately twice that of the cooling demand. The average daily solar irradiation is approximately 3.5–3.6 kWh/m^2/day, peaking around the spring equinox and reaching its minimum around the winter solstice. Annual precipitation is about 1,100–1,400 mm and is concentrated mainly in the June–September period. These climatic characteristics were used in the thermal analysis to predict the annual energy consumption. We employed typical meteorological year weather data for Seoul provided by the International Weather for Energy Calculation dataset [51].

To evaluate the thermo-optical performance of the HSC_W test specimens, we used values taken from test certificates issued by the Korea Conformity Laboratories, an accredited testing agency. The HSC_W specimens were fabricated with horizontal PV cells embedded in polydimethylsiloxane. Because the horizontal arrangement of the PV cells led to a non-homogeneous assembly, a separate thermal resistance test was required. In accordance with the test standards, a specimen size of 300 mm × 300 mm was used for thermal resistance testing and 100 mm × 100 mm specimens were employed for thermo-optical testing. Hereafter, "HSC" is used to denote the individual glass elements in the window, while "HSC_W" denotes the final window system as an insulating glass unit. To verify the thermo-optical performance of the

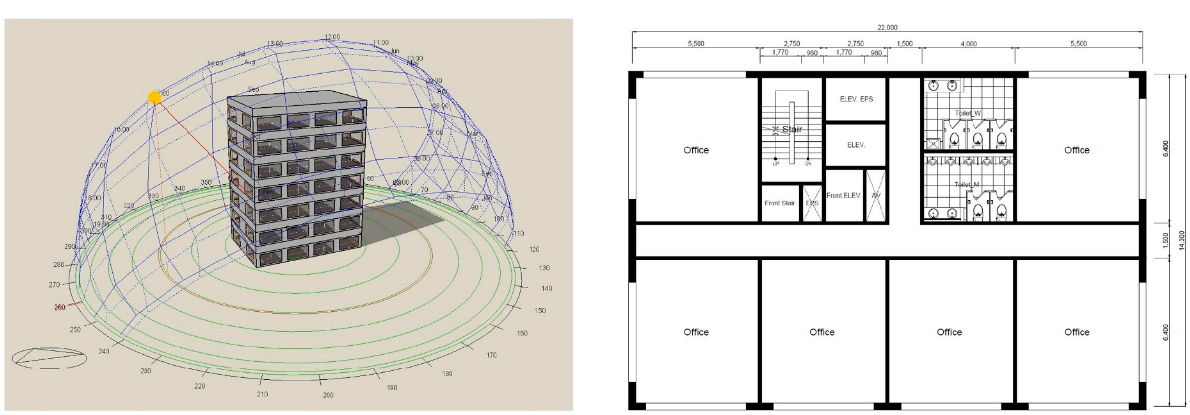

(a) Exterior modeling (b) Office floor plan for the target building

Fig. 4. Overview of the simulation model.

Table 2
Input parameters for the simulation model.

Component	Parameter	Information
Building summary	Location	Seoul, South Korea
	Latitude/longitude	37.56 N/127.98 W
	Climate zone	4A (mixed humid climate)
	Building type	Office medium
	Total floor area	314.6 m^2
	Ceiling height	2.8 m
	Window-to-wall ratio	45 %
U-value	Infiltration	1.5 ACH
	Roof	0.150 W/m^2·K
	External wall	0.240 W/m^2·K
	Ground floor	0.290 W/m^2·K
	Window	1.500 /m^2·K
Interior heat gain	Occupancy	18.58 m^2/people
	Office equipment	8.07 W/m^2
	Lighting	Office 400 lx Core 200 lx
	Lighting control	Linear off
HVAC	System	VRF (DOAS)-DCV
	Heating/cooling fuel	Electricity from the grid
	Heating/cooling COP	4.0/4.2
	Heating setpoint/ setback	20.0°C/26.0°C
	Cooling setpoint/ setback	15.5°C/29.4°C
	Heating period	January 1 to April 30, October 1 to December 31
	Cooling period	May 1 to September 30

finished product, we conducted thermo-optical measurements and thermal resistance testing on the HSC_W layer configuration.

The tests followed the methods KS L 2514, KS L 2525, and KS L 9016, through which we evaluated 13 thermo-optical properties: VLT, inside/outside visible reflectance, solar transmittance, inside/outside solar reflectance, infrared transmittance, inside/outside transmittance, U-value, emissivity, SHGC, and thermal resistance. In addition, the shading coefficient (SC) was measured in accordance with NFRC 300:2017. Across the four test methods, we obtained 14 variables (Table 3). Both the cell efficiency and the module efficiency applied in this study were obtained from the I–V measurement system provided by Chungbuk Technopark.

The measured properties were used to construct the simulation window models by entering the glass data in DesignBuilder, which is based on the International Glazing Database (IGDB). IGDB contains glazing product information from approximately 2,500 manufacturers worldwide and is an international standard database compatible with the WINDOW 6 software developed by Lawrence Berkeley National Laboratory [52,53]. Following ASHRAE recommended calculation procedures, we used DesignBuilder to calculate the U-value, VLT, SHGC, and SC (Table 4). Both windows satisfied the current legal limit of 1.5 W/m^2·K, and the properties of the Low-e window were based on certified test values for a commercial product [54].

Table 3
Physical properties of the HSC_W cells.

Parameter	Value
Glazing layer thickness (mm)	24.0
U-value (W/m^2·K)	3.83
Solar heat gain coefficient	0.80
Shading coefficient	0.91
Visible reflectance (%)	90.0
Inside/outside visible reflectance (%)	8.0/7.9
Solar transmittance (%)	73.3
Inside/outside solar transmittance (%)	7.1/7.0
Infrared transmittance (%)	56.9
Inside/outside infrared transmittance (%)	6.2/6.1
Emissivity	0.84
Thermal resistance (m^2K/W)	0.087

4. Results and discussion

4.1. Reliability verification

4.1.1. Base model reliability verification

The simulation reference building was configured based on ASHRAE, Korea's Building Energy Saving Design Standards, prior studies, and statistical data. To verify the reliability of the simulation target, we compared its electricity use with that of buildings with a similar completion year, use, and gross floor area. Actual electricity consumption data were obtained from the Architecture HUB portal operated by the Ministry of Land, Infrastructure and Transport, a digital platform that integrates building-related datasets and provides detailed building information and monthly electricity use with filters by region, year of completion, structure, use, and number of stories [55].

To assemble a statistically meaningful sample, we considered the gross floor area, region, completion year, and primary use. The sample was limited to office buildings located in Seoul, Republic of Korea. To reflect differences in the heat source type and major systems, we targeted mid-size buildings with a floor area of 500–3,000 m^2 [56]. To account for the introduction of stronger insulation standards, the completion year was restricted to 2017 or later.

Real buildings vary widely in their structure, occupancy, WWR, and orientation; therefore, we employed the energy use intensity (EUI, kWh/m^2·yr) as the evaluation metric, defined as the annual final energy consumption per unit of floor area (Eq. (1)). The sample consisted of 61 buildings with an EUI ranging from 34.3 to 135.4 kWh/m^2·yr (mean: 82.7 kWh/m^2·yr). The simulation target building had seven stories and a floor area of 2,202.2 m^2 with Low-e glazing. Fig. 5 presents a box plot comparison of the EUI for the simulation model and the sample. The box spans the interquartile range (IQR; 25 %–75 %), and the × symbol denotes the mean. Outlier thresholds were set at 1.5 × the IQR from the 25 % and 75 % points. The EUI of the simulation model was 71.7 kWh/m^2·yr, which was within the IQR, indicating that the target building's energy use was reliable. The slightly lower EUI of the target relative to the sample likely reflected the inclusion of elevator and base loads in the comparison sample.

$$EUI = \frac{Energy\ consumption\ (kWh)}{Floor\ area\ (m^2)} \quad (1)$$

4.1.2. Mock-up and simulation reliability verification

To ensure the validity of the simulation analysis, we performed reliability verification using the mock-up measurements as the reference. Unlike conventional commercial PV modules, the HSC_W system is constructed by cutting PV panels into fixed sizes and modularizing them; therefore, standardized nameplate generation data do not exist. Before the simulation-based analysis, we compared the actual PV generation measured in the mock-up installation with the simulated results to confirm their validity. PV generation for the HSC_W system was

Table 4
Composition and physical properties of the HSC_W and Low-e window.

Window Type	Layer (thickness)	U-Value (W/m^2·K)	SHGC	SC	VLT (%)	Eff (%)
Low-e	Clear glass (6 mm) + Argon layer (16 mm) + Low-e glazing (6 mm)	1.25	0.59	0.56	66.1	-
HSC_W	HSC array (22 mm) + Argon layer (13 mm) + Low-e glazing (6 mm)	1.27	0.35	0.45	39.2	22.6

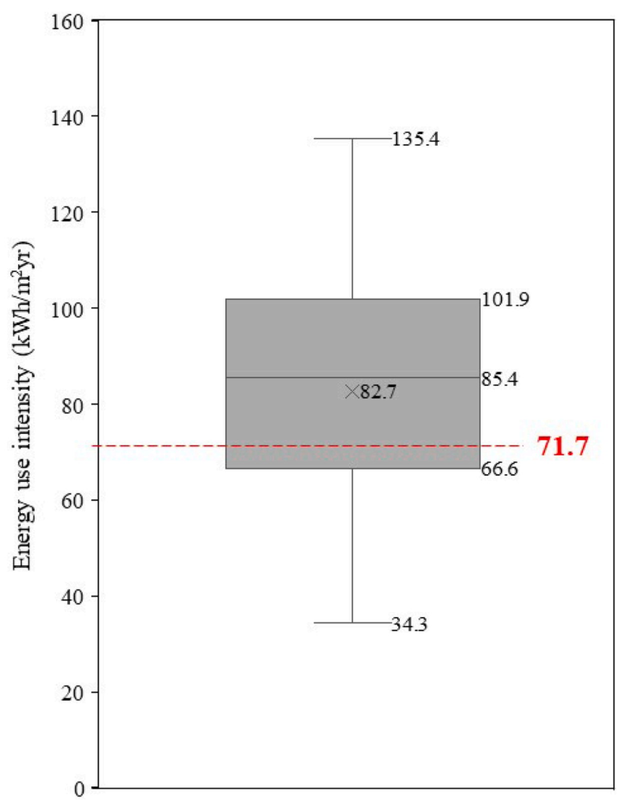

Fig. 5. EUI box plot for base model validation.

simulated using DesignBuilder. Because the minimum PV cell height in DesignBuilder is limited to 30 mm, the actual mock-up cell height of 0.79 mm could not be modeled directly [57]. To compensate for this, we adjusted the scale of the model and then conducted the simulation so that the results approximated the real mock-up conditions.

We refer to the model before scaling as the "authentic" model and that after scaling as the "simulation" model. To predict the PV generation in the mock-up environment, the PV values obtained from the simulation model were corrected using the area ratio relative to the authentic model (Eq. (2)). The power generation calculated from the PV using this scale factor was then divided by the same scale factor to estimate the power generation under real conditions, thus overcoming the modeling limitations of DesignBuilder and reflecting the actual PV cell design (Eq. (3)):

$$Scale\ Factor = \frac{Authentic}{Simulated} \tag{2}$$

$$P_{corr} = \frac{P_{DB}}{SF} \tag{3}$$

where P_{corr} is the corrected electricity generation (kWh), P_{DB} is the electricity generation calculated in DesignBuilder (kWh), and SF is the scale factor.

Although the PV cell thickness was scaled up to 30 mm due to the minimum resolution limits of DesignBuilder, this adjustment was applied solely to the PV power calculation. All thermo-optical properties, including the SHGC, VLT, U-value, reflectance, emissivity, and thermal resistance, were directly input using certified laboratory measurements rather than values derived from the scaled geometry. Furthermore, the scaled simulation results were validated using the mock-up measurements, yielding a normalized mean bias error (NMBE) of 3.5 %, which satisfied the ASHRAE Guideline 14 tolerance. Therefore, the scaling procedure did not introduce meaningful errors to the simulation.

As the reliability metric, we used the NMBE, which directly evaluates the systematic bias between predictions and measurements. Compared with the root mean square error and the coefficient of variation of the root mean square error, NMBE offers a clearer interpretation of bias and is recommended by ASHRAE Guideline 14 and the IPMVP for the verification of simulations. By normalizing the error by the measured mean, NMBE also allows for a comparison of different magnitudes of power generation, which is useful for PV verification, where output varies by installation and environment [58–60]. Eq. (4) was used to calculate the NMBE:

$$NMBE = \frac{\sum_{k=1}^{n}(y_k - \hat{y}_k)}{\sum_{k=1}^{n} y_k} \times 100(\%) \tag{4}$$

where y and $\hat{y}$ represent the simulation and measurement results, respectively. ASHRAE Guideline 14 allows an NMBE of ±10 % for time-series data. Our NMBE was 3.5 %, indicating that the PV generation measured in the mock-up environment exceeded that determined in the simulations; nevertheless, it fell within the allowable tolerance, confirming that the model adequately represented the power generation performance of HSC_W.

4.2. Mock-up experimental results

4.2.1. Indoor light and thermal environment

Fig. 6 presents the vertical solar irradiance and indoor illuminance by window type over the measurement period. Both window types exhibited similar temporal patterns in response to irradiance; however, the Low-e window consistently produced higher illuminance than the HSC_W, with the difference becoming more pronounced on clear, high-irradiance days. Overall, indoor illuminance with the HSC_W was approximately 48–52 % lower than that of the Low-e window, and the maximum difference during peak irradiance hours reached about 7,800 lx. For both window types, indoor illuminance increased from October to December as the solar altitude decreased. Maximum illuminance occurred on December 22 (16,116.2 lx for the Low-e window and 8305.1 lx for the HSC_W), while the minimum occurred on October 23 (371.8 lx and 177.5 lx, respectively). These results indicate that the insertion of PV cells into the HSC_W reduced the VLT and, consequently, the indoor illuminance.

In terms of thermal performance, the U-values were 1.25 W/m^2·K for the Low-e window and 1.27 W/m^2·K for the HSC_W, representing only a 1.8 % difference in insulation performance. Fig. 7(a,b) summarizes the daily mean outdoor temperature, indoor air temperature, and front and rear glass temperatures for both window types. The front glass of the HSC_W was consistently warmer than that of the Low-e window, with average differences of 1.7°C in October, November, and December. This was attributed to the fraction of absorbed solar energy that was not converted into electricity but dissipated as heat, which was approximately 78–85 % given typical PV efficiencies. In contrast, the rear-glass temperature of the Low-e window was higher (by 1.2–1.4°C) because its higher SHGC (0.59) allowed more solar heat to enter the indoor environment than the HSC_W (0.38).

The indoor air temperature was generally about 0.8°C higher in the space with Low-e glazing, with monthly means for October, November, and December of 20.0°C, 13.0°C, and 4.0°C, respectively, compared with 19.2°C, 12.1°C, and 3.2°C for HSC_W, respectively. The higher SHGC of the Low-e glazing admitted more solar heat, raising the indoor temperature, whereas HSC_W reduced indoor heat via PV absorption and electrical conversion. This would be a benefit for reducing the cooling load in summer but may increase the heating energy demand in winter. In the mock-up, however, radiant effects from the glass were moderated by natural ventilation through the rear ventilation opening and by convection, so the differences in the indoor temperature were modest. Overall, HSC_W functions as a hybrid window system that both generates electricity and affects the thermal performance of the

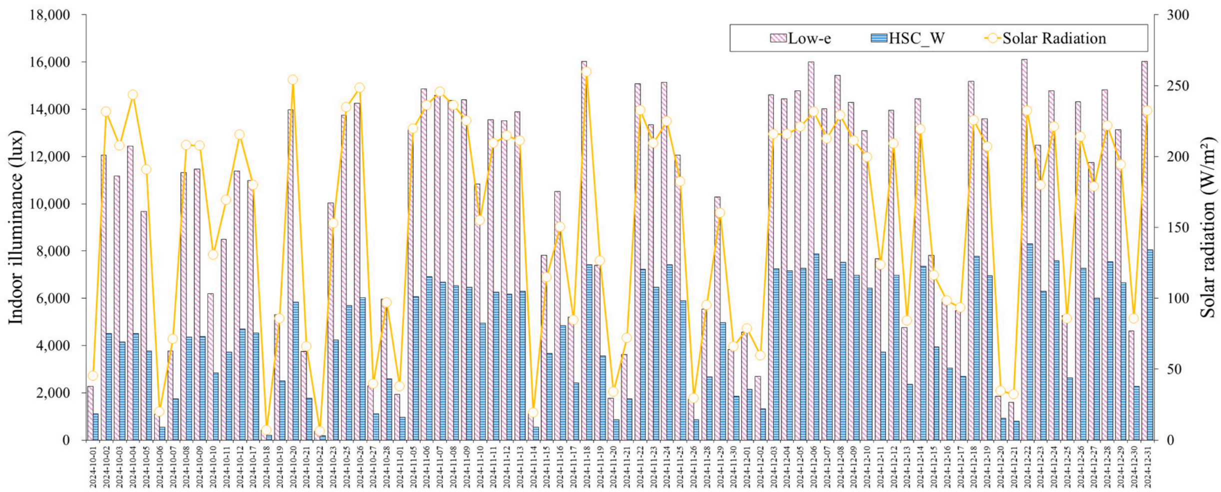

Fig. 6. Daily indoor illuminance and vertical solar irradiance for HSC_W and Low-e windows.

building. Because the seasonal impact of the SHGC differs, the selection of window systems should consider building use and local climate characteristics.

4.2.2. PV generation measurements

Fig. 8 presents the daily means for the vertical irradiance and PV generation observed during the winter test period (October–December). During this period, the mean vertical irradiance increased from 144.9 W/m^2 in October to 155.4 W/m^2 in November and 168.7 W/m^2 in December (+16.4 % from Oct to Dec), whereas the mean daily PV generation decreased from 68.3 Wh to 45.4 Wh and 37.7 Wh in the same months (−44.8 %). Although PV systems generally exhibit a positive correlation between solar irradiance and power generation, the inverse trend observed in the present study was attributable to seasonal characteristics specific to the winter test period. The experiment was conducted during a time of short daylight hours, a low solar altitude, and an increased incidence angle, all of which limited the effective insolation and reduced the conversion efficiency of the vertically installed HSC_W. In addition, frequent cloudy conditions and partial shading led to low-light operation and string mismatch losses, contributing further to the reduced power generation. Therefore, these findings reflect seasonal constraints inherent to the winter-only dataset rather than the long-term performance of the system. Indeed, the annual simulation results demonstrated the expected positive correlation between irradiance and PV generation, with noticeably higher generation during the summer when the daylight hours and solar altitude increased.

The PV generation measured for HSC_W was lower than the manufacturer's reported nominal efficiency. This was attributed to a decrease in the incidence angle modifier (IAM) with seasonal changes in the solar altitude, a reduction in the effective aperture area arising from cutting the cells into fixed sizes and arranging them in the window system, and partial shading and string mismatch effects, which are characteristic of façade-integrated PV systems. These structural characteristics must be considered in the implementation of HSC_W as a BIPV system, while improvements in PV efficiency are also required by optimizing the cell components and accounting for seasonal variability.

4.3. Computer simulation results

Based on the simulation model validated in Section 4.1.1, this study analyzed the indoor environmental and energy performance of the HSC_W system and Low-e glazing windows. This analysis focused on daylighting and thermal conditions, energy consumption, and PV generation, with the reliability of the PV generation estimates established through a comparison with the mock-up experimental data. By varying the VLT and SHGC of the two window types, we quantitatively evaluated the daylighting performance and solar heat gains and consequently determined the expected energy-saving effects for real building applications.

4.3.1. Evaluation of light and thermal environment performance

The daylighting performance of HSC_W was evaluated using indoor illuminance and daylighting metrics, while thermal conditions were monitored according to changes in the indoor air temperature due to solar heat gains. The reference room was south-facing, on the fourth floor, and in the central zone, where the influence of the external environment was minimized and building-to-building distance effects could be avoided. Artificial lighting was also excluded, with only natural light entering through the windows considered. The illuminance for each window type was evaluated under CIE overcast sky conditions, with the indoor illuminance measurement points set at a working plane height of 0.8 m. Furthermore, to determine the potential domestic and international applicability of the proposed HSC_W system, its performance was compared with the daylighting performance standards established by the domestic and international ecofriendly building certification systems LEED, BREEAM, and G-SEED. LEED v4.1 evaluates annual daylighting performance using spatial daylight autonomy (sDA300/50 %) and annual sunlight exposure (ASE1000, 250), requiring that the proportion of the floor area satisfying $\geq$ 300 lx for more than 50 % of the occupancy time be at least 55 % [61]. BREEAM requires an average daylight factor (DF) of 2 % or more and a uniformity ratio (UR) of 0.3 or more [62], while G-SEED evaluates compliance with a reference illuminance for particular uses [63].

The analysis results revealed that neither window met the floor area within limits (FAWL) criterion used by LEED, which requires $\geq$55 % of the floor area to be within the illuminance standard range (43.5 % for Low-e windows and 29.3 % for HSC_W). The Low-e windows met BREEAM's requirement of an average DF of $\geq$2 % (3.58 %), while HSC_W was only slightly below this standard (1.99 %). Similarly, the average illuminance of the Low-e windows was close to the standard range for G-SEED's appropriate illuminance standards for office buildings [64], but HSC_W had a low average illuminance and did not meet the standard. Both the Low-e windows and HSC_W failed to reach the LEED minimum illuminance standard of 300 lx (59.6 and 33.9 lx, respectively) and the BREEAM uniformity ratio standard of $\geq$0.3 (0.16 and 0.17, respectively), but both met the LEED maximum illuminance standard of $\leq$2,000 lx (1,874.0 and 1,003.0 lx, respectively).

The limited performance of HSC_W compared to these international certification standards was attributed to its limited illuminance due to the low VLT of the proposed design (39.3 %). This means that additional

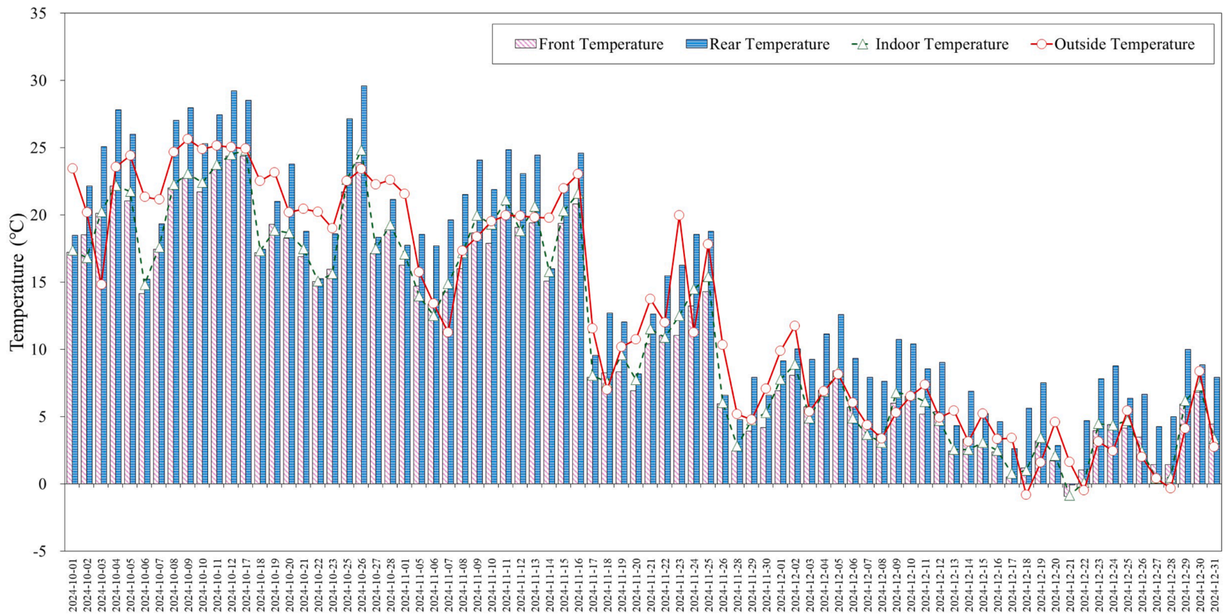

(a) Surface and indoor air temperatures for the Low-e window.

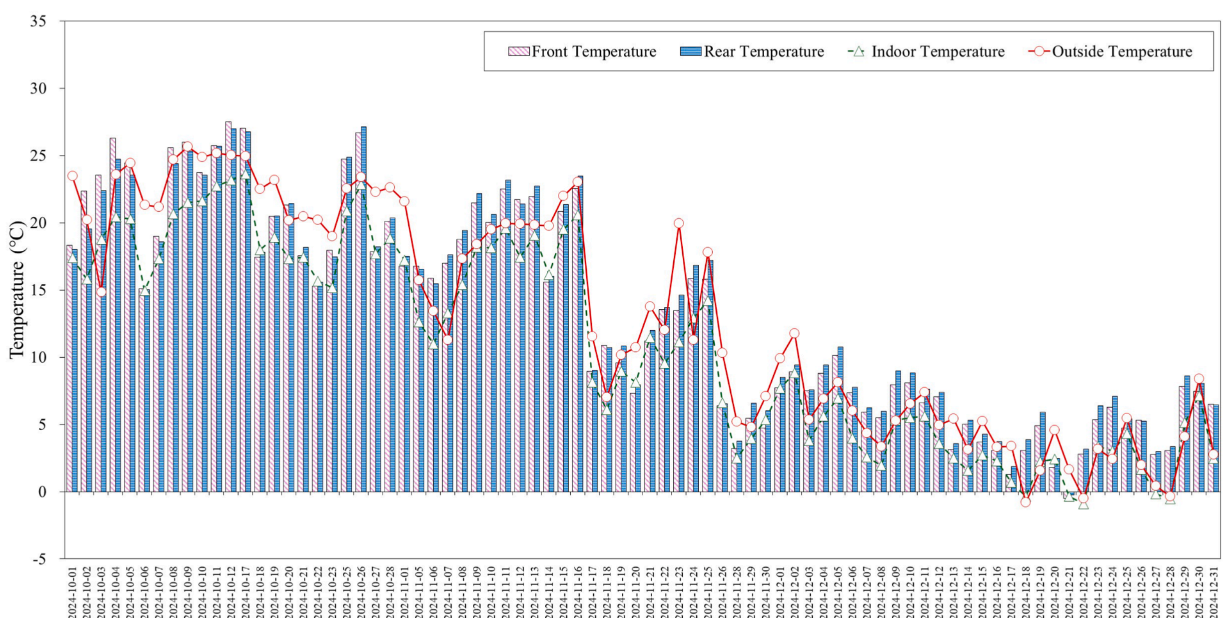

(b) Surface and indoor air temperatures for HSC_W.

Fig. 7. Daily front and rear surface temperatures and indoor air temperatures by window type.

artificial lighting systems are needed when used in actual buildings. In particular, for HSC_W, the decrease in the VLT due to the presence of the solar cells directly affects its lighting energy consumption, creating a direct tradeoff between PV generation and indoor illuminance. Therefore, when employing HSC_W, it is necessary to improve its daylighting performance by raising both its VLT and PV efficiency. However, because HSC_W simultaneously generates power via its solar cells, careful assessment of both its additional lighting energy requirements and PV generation is necessary when determining its utility.

We also examined the effect of the glazing thermal properties of HSC_W on the indoor thermal environment. Thermal performance was evaluated based on the solar heat gain and resulting changes in the indoor air temperature. The solar heat gain is primarily governed by the SHGC of the glazing, with a higher SHGC generally admitting more solar heat. To isolate the effects of the glazing, simulations were conducted with the HVAC system and electric lighting turned off. The resulting analysis found that Low-e glazing produced a substantially higher solar heat gain due to its relatively high SHGC compared to HSC_W, with an annual total solar heat gain of 4,382.7 kWh and 1,347.8 kWh, respectively, a difference of 225 %. Both window types experienced the highest solar heat gain in winter (December–February), when the solar altitude is low, and the lowest in summer (June–July) (Fig. 9). In January, low-e glazing had a maximum solar heat gain of 544.7 kWh, while that of HSC_W was 167.5 kWh, a difference of 30.8 %.

Despite the large disparity in the solar heat gain between the two window types, the differences in the indoor air temperature were relatively modest. The annual average indoor air temperature was 23.4°C for low-e glazing and 21.8°C for HSC_W, rising to 32.5°C and 30.8°C, respectively, in summer (June–August) and falling to 14.5°C and 10.4°C, respectively, in winter (December–February). The smaller difference in

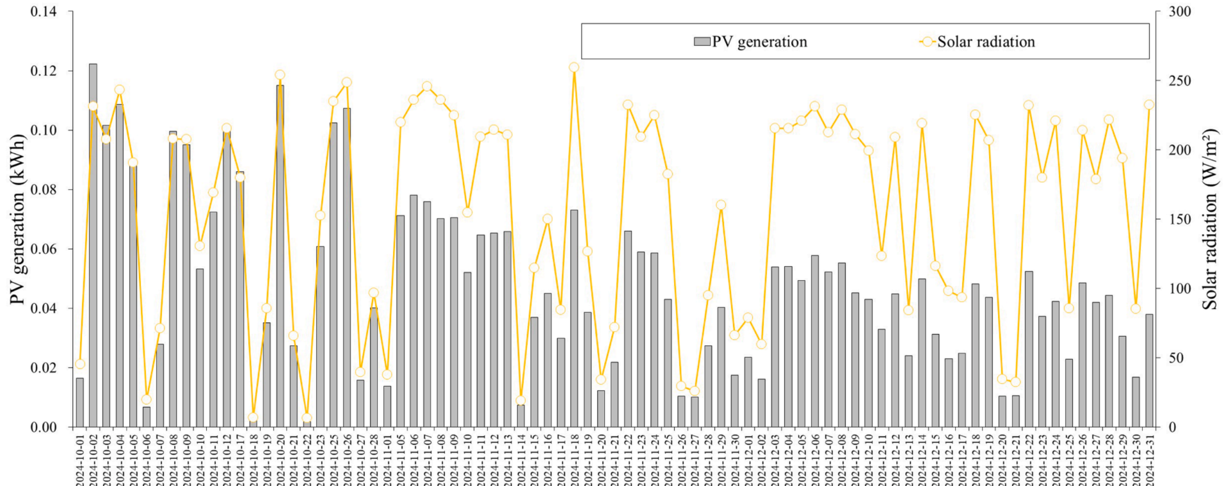

Fig. 8. Daily means for the vertical solar irradiance and PV generation of HSC_W.

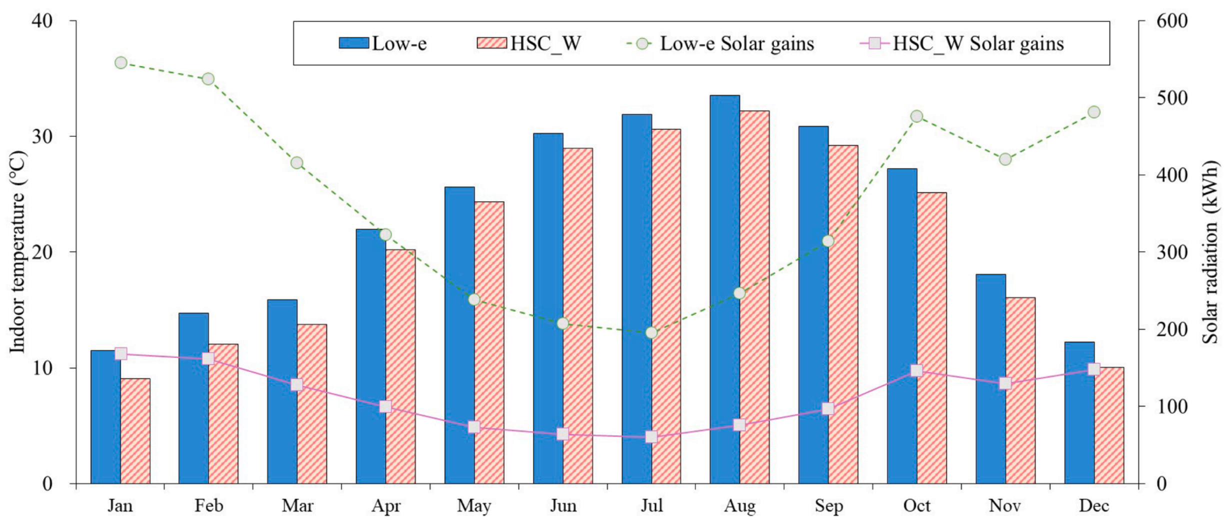

Fig. 9. Monthly indoor air temperature and direct solar radiation profiles for the reference room.

the indoor temperature was attributed to the combined effects of the boundary conditions (e.g., no HVAC operation and the exclusion of ventilation and internal heat gain) and the buffering effect of the structural thermal mass of the building. In addition, the difference in the U-value between the two windows was only ~0.002 W/m^2·K, suggesting that the SHGC had a greater impact on the thermal environment.

Overall, the indoor daylighting and thermal environment analysis clearly highlighted the differences in the performance characteristics and potential applications of the two window types. Low-e glazing, with its high VLT (66.1 %) and SHGC (0.590), offers excellent natural lighting performance and winter solar heat gain, while HSC_W, with its relatively low VLT (39.3 %) and SHGC (0.383), has limited daylighting performance but provides multifunctional capabilities, including a reduction in the summer cooling load and simultaneous electricity generation. In particular, the low SHGC of HSC_W acts as a key factor maximizing its energy-saving effect in office buildings where cooling loads are dominant, which is an important advantage when considering domestic climate characteristics and building functions. Therefore, window selection should consider the building purpose, regional climate, and annual energy demand patterns rather than individual performance indicators. To ensure the practical use of novel window systems such as HSC_W, improvements in the VLT to meet daylighting performance standards for domestic and international certification systems should be accompanied by optimization strategies for the thermal performance in response to seasonal changes in solar radiation.

4.3.2. Building energy consumption

Korea's ZEB certification evaluates the energy used for heating, cooling, domestic hot water (DHW), lighting, and ventilation [9]. However, under Korea's regulations for building equipment standards, ventilation energy is excluded for office buildings with a gross floor area below 3,000 m^2 [65], while DHW use is driven by occupant schedules and is independent of the window type. Accordingly, we focused on the use of energy for heating, cooling, and lighting in our analysis of the building energy consumption when using the Low-e windows and HSC_W. The proposed HSC_W system had an annual energy consumption of 60,192.9 kWh, approximately 1.3 % lower than that of the Low-e windows (61,000.7 kWh). However, when broken down by specific uses, the heating and lighting energy was approximately 9.5 % and 6.0 % higher for HSC_W, while the cooling energy was 14.6 % lower, confirming its energy-saving effect for cooling. The higher heating and lighting energy consumption when using HSC_W was attributed to the lower solar heat gain due to its low SHGC and reduced natural light due to its low VLT.

Monthly analysis revealed that the cooling energy reduction due to HSC_W was particularly pronounced during summer (June–August)

(Fig. 10). In August, the Low-e windows required 6,722.4 kWh, while HSC_W used 5,882.6 kWh, a reduction of approximately 12.4 %. This resulted from the substantially lower solar radiation entering the room due to the low SHGC. Conversely, during winter (December–February), the heating energy consumption was expected to increase sharply due to the lower solar heat gain, but the analysis found that the increase in the heating energy consumption was relatively small. This was likely because the target building had a high cooling load ratio, and the cooling energy savings due to the blocking of solar radiation by HSC_W offset the increase in the heating energy. Therefore, despite HSC_W having a lower SHGC and VLT than the Low-e windows, it achieved a 1.3 % reduction in total energy consumption. This analysis thus suggests that the proposed HSC_W system may be suitable for domestic office buildings with high cooling load ratios, and its energy-saving effects could be further enhanced by combining it with highly efficient lighting and dynamic shading systems to address the higher lighting energy requirements due to its lower VLT.

4.3.3. PV generation and net energy consumption

We also analyzed the net energy consumption to account for PV generation by the HSC_W system. EnergyPlus was used to compute panel-level PV generation based on PV efficiency and solar radiation, while considering the panel temperature, tilt, weather conditions, and orientation [66]. Although the same window size (4.32 m × 2.20 m) was used for all orientations, the number of windows on each facade differed. Annual PV generation was highest for the south orientation, followed by, in order, the east, west, and north orientations. The south facade had a monthly maximum of 893.12 kWh in March and 864.72 kWh in October due to the optimal solar altitude and higher direct solar radiation during these months. The east and west orientations had similar PV generation patterns, reaching approximately 70–80 % of that of the south orientation. The north orientation had the lowest annual generation (585.64 kWh/yr) due to limited direct solar radiation and reliance on diffuse solar radiation. In particular, the direct solar radiation peaked at 167.7 W/m^2 in April and 143.7 W/m^2 in October, while the diffuse solar radiation remained relatively constant in the 60–80 W/m^2 range throughout the year.

Table 5 lists monthly energy consumption, PV generation, and net energy consumption for the proposed HSC_W system. Noticeable differences in the monthly net energy consumption were observed, with net energy consumption tending to be higher in summer (June–August) and winter (December–February) due to cooling and heating loads, respectively, reaching 8,480.4 kWh in August and 8,032.2 kWh in January. Conversely, relatively low energy consumption was recorded in April–May and Oct–Nov. PV generation peaked in February–May and September–October, with March producing the annual maximum (1,326.5 kWh). The lower power generation in summer and winter was attributed to the lower solar cell efficiency arising from high temperatures and sunshine hour limitations, respectively.

Table 5
Monthly energy consumption, PV generation, and net energy consumption for the HSC_W system.

Month	Total energy consumption	PV generation	Net energy consumption
Jan.	8,480.4	891.9	7,588.5
Feb.	5,684.7	1,134.2	4,550.6
Mar.	4,293.2	1,326.5	2,966.7
Apr.	2,022.4	1,204.1	818.3
May	2,690.7	1,025.4	1,665.3
Jun.	4,658.1	935.3	3,722.8
Jul.	7,024.8	806.9	6,217.9
Aug.	8,032.2	950.3	7,081.9
Sep.	4,818.5	1,052.6	3,765.8
Oct.	1,512.0	1,234.2	277.8
Nov.	3,785.5	762.0	3,023.5
Dec.	7,190.6	742.9	6,447.7
Total	60,192.9	12,066.2	48,126.7

The contrasting seasonal patterns observed for energy consumption and PV generation directly influenced the net energy consumption. The annual net energy consumption for HSC_W was calculated to be 48,126.7 kWh, indicating that PV generation could reduce the energy consumption by approximately 21.1 % compared to the Low-e window system (Fig. 11). The monthly energy offset also exhibited distinct seasonal variation. For example, in April, 1,204.1 kWh of the total energy consumption of 2,022.4 kWh was replaced by PV generation, representing an offset rate of 59.5 %, while October recorded the maximum offset rate (81.6 %; 1,234.2 kWh from a total of 1,512.0 kWh). This was the result of smaller cooling and heating loads during the spring and fall seasons, while the solar altitude and weather conditions optimized the efficiency of PV generation. In contrast, the energy offset effects of PV generation were limited during the December–January and July–August periods when the cooling and heating loads were higher (10.5 % and 11.8 % in January and August, respectively).

Total energy consumption exhibited a complex pattern due to the conflicting effects of the seasonal energy demand and PV generation. Although PV generation reduced the annual energy consumption by approximately 21.1 % compared to the Low-e windows, this was insufficient to fully cover the building's total energy demand. This suggests that the PV generation performance of HSC_W alone cannot meet the building's total energy consumption during periods when

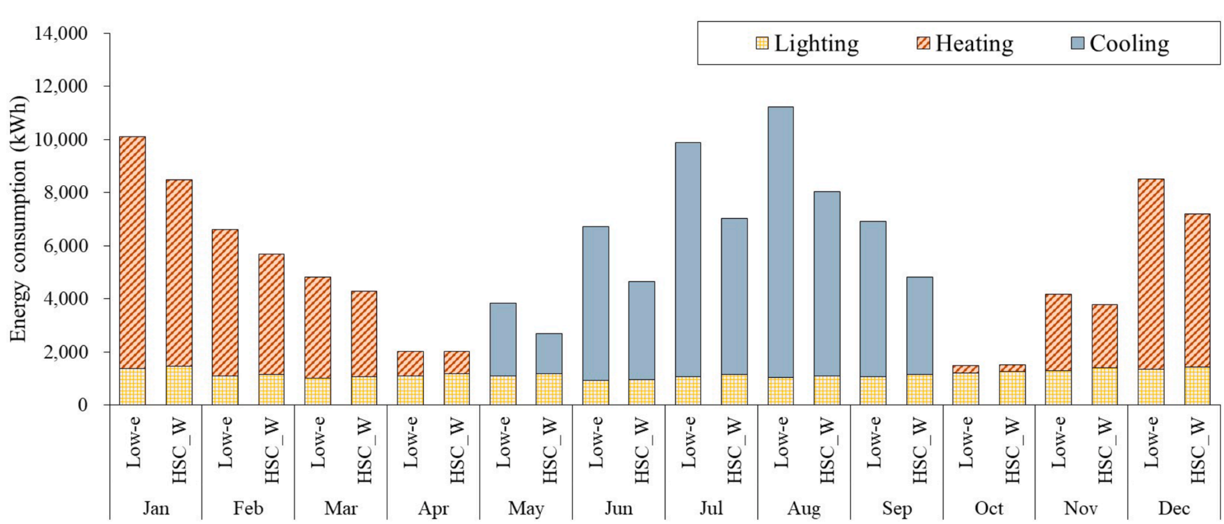

Fig. 10. Monthly heating, cooling, and lighting energy consumption for the HSC_W and Low-e window.

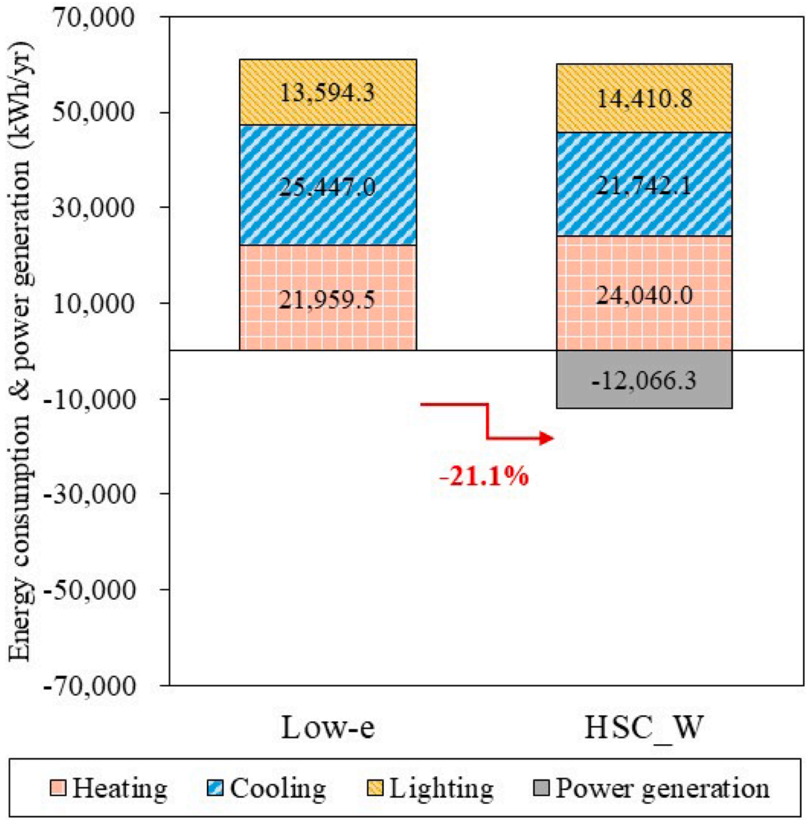

Fig. 11. Building energy consumption by heating, cooling, lighting, and PV generation.

cooling or heating demand is high.

4.3.4. *ZEB feasibility assessment*

The results of the PV generation and net energy consumption analysis indicated that the thermo-optical performance of the HSC_W system needed to be optimized to achieve energy independence for the target building. This is because the thermo-optical properties of windows directly affect lighting, cooling, and heating loads. In particular, in buildings with large cooling loads, such as office buildings, changes in the VLT and SHGC have a pronounced influence on the total energy demand. Therefore, the optimal combination of the VLT and SHGC was assessed in order to evaluate the feasibility of the proposed system achieving ZEB Grade 5 criteria.

To assess compliance with the ZEB Grade 5 requirements, the energy independence of each window configuration was evaluated using the ESSR. In this study, the ESSR was defined as the ratio of the annual renewable energy generation to the annual primary energy consumption, expressed as a percentage. The electricity generated by the HSC_W system was converted into primary energy using a conversion factor of 2.75, in accordance with the national ZEB certification framework. This approach enabled a consistent comparison of ESSR values between different thermo-optical configurations, thus determining whether each case satisfied the minimum energy self-sufficiency required for ZEB Grade 5.

The baseline properties of HSC_W (VLT: 39.3 %; SHGC: 0.383) were approximately 40 % and 35 % lower, respectively, than those of Low-e windows (VLT: 66.1 %; SHGC: 0.590) due to the presence of the solar cells. Accordingly, we set Low-e windows as the base model and analyzed the energy-saving effects for nine versions of HSC_W with different combinations of the VLT and SHGC (Table 6). We calculated the ESSR based on current office building standards and assessed the possibility of achieving ZEB Grade 5 for each case. The tested VLT–SHGC combinations were set to gradually improve the performance gap

Table 6
VLT–SHGC combinations for HSC_W.

Case	VLT	SHGC
Case 1	40 %	0.4
Case 2	40 %	0.5
Case 3	40 %	0.6
Case 4	50 %	0.4
Case 5	50 %	0.5
Case 6	50 %	0.6
Case 7	60 %	0.4
Case 8	60 %	0.5
Case 9	60 %	0.6

between HSC_W and Low-e windows. In particular, the VLT was set to 40 %, 50 %, and 60 %, while the SHGC was set to 0.4, 0.5, and 0.6. These values also reflected the range recommended in Korea's Building Energy Saving Design Standards (0.4–0.6) and the cooling load characteristics of office buildings [38].

The simulation results revealed that the total energy consumption varied by up to 2.73 % depending on the VLT–SHGC combinations (Fig. 12). Relative to Low-e windows, Case 7 (VLT: 60 %; SHGC: 0.4) achieved the best performance with a 2.27 % reduction, while Cases 2 (VLT: 40 %; SHGC: 0.5) and 9 (VLT: 60 %; SHGC: 0.6) had minimal reduction effects of 0.05 % and 0.46 %, respectively. Conversely, Case 3 led to a 1.51 % increase, which was the only case where energy consumption increased compared to the base model. Analysis by energy type found that the heating energy consumption tended to increase for all HSC_W combinations compared to the base model, which was attributed to the lower solar heat gain due to the low SHGC. In contrast, the cooling energy consumption decreased for most of the combinations, though the degree of change was limited. The cooling energy requirements actually increased for Cases 3 (VLT: 40 %; SHGC: 0.6), 6 (VLT: 50 %; SHGC: 0.6) and 9 (VLT: 60 %; SGHC: 0.6) due to their high

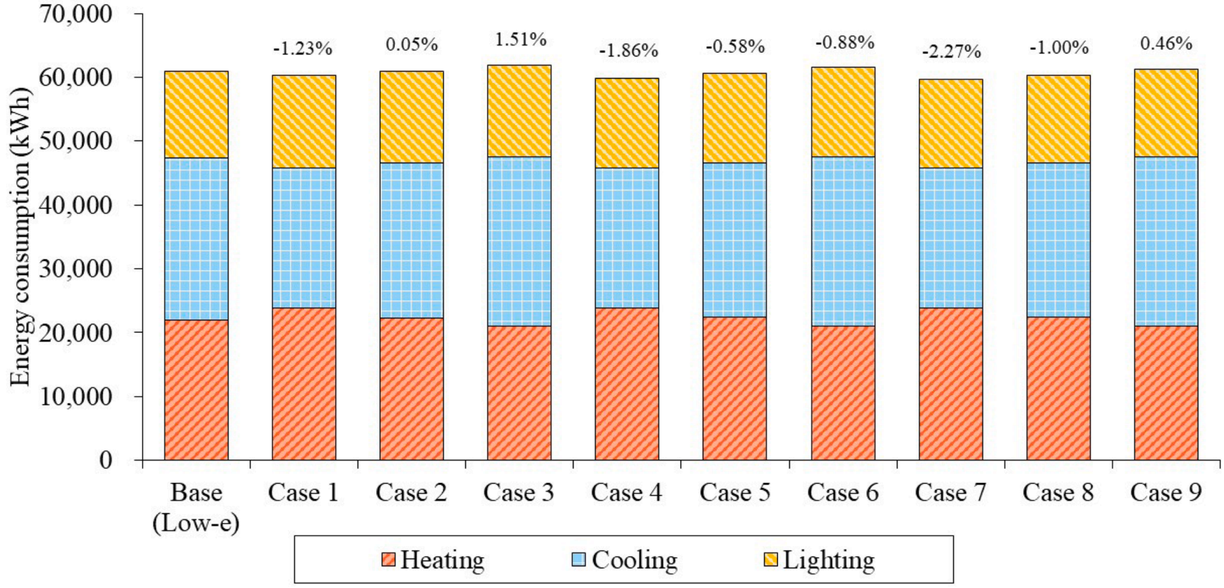

Fig. 12. Energy consumption for different VLT–SHGC combinations using HSC_W and percentage difference compared to Low-e windows.

SHGC. Lighting energy consumption tended to decrease with a higher VLT, with Cases 7 (VLT: 60 %; SHGC: 0.4), 8 (VLT: 60 %; SHGC: 0.5), and 9 (VLT: 60 %; SHGC: 0.6) having the largest reduction effect.

To evaluate the possibility of achieving ZEB Grade 5, the ESSR was calculated for each combination. Based on an annual PV generation of 12,066.2 kWh achieved by HSC_W, Cases 4 (VLT: 50 %; SHGC: 0.4) and 7 (VLT: 60 %; SHGC: 0.4) achieved the highest ESSR (20.2 %), while Case 3 (VLT: 40 %; SHGC: 0.6) had the lowest ESSR (19.5 %; Fig. 13). Overall, four combinations (Cases 1, 4, 7, and 8) met Korea's ZEB Grade 5 standards (ESSR $\geq$20 % and <40 %).

These results confirmed that VLT and SHGC had opposing effects on the building energy consumption. While a higher VLT reduced the lighting energy consumption, an increase in the SHGC raised the cooling energy required, adversely affecting the overall performance. The optimal combinations were Cases 4 and 7, which were able to maximize natural lighting while minimizing the cooling load. This demonstrated that HSC_W can improve building energy performance while maintaining sufficient PV generation by optimizing its thermo-optical properties, with its practical applicability highlighted by its ability to meet ZEB Grade 5 standards for selected combinations of the VLT and SHGC. Although the energy savings of the optimal combinations were limited, using the proposed HSC_W system in office buildings with a high WWR can contribute to improving the ESSR and achieving ZEBs.

5. Conclusions

This study aimed to evaluate the indoor thermal performance, daylighting performance, and PV generation characteristics of an HSC_W system through full-scale mock-up experiments combined with building energy simulations. The mock-up measurements were taken to observe the thermo-optical behavior and PV output of the system, while annual heating and cooling loads and electricity production were assessed through simulations. Furthermore, the effects of varying the VLT and SHGC of the HSC_W were examined by configuring multiple

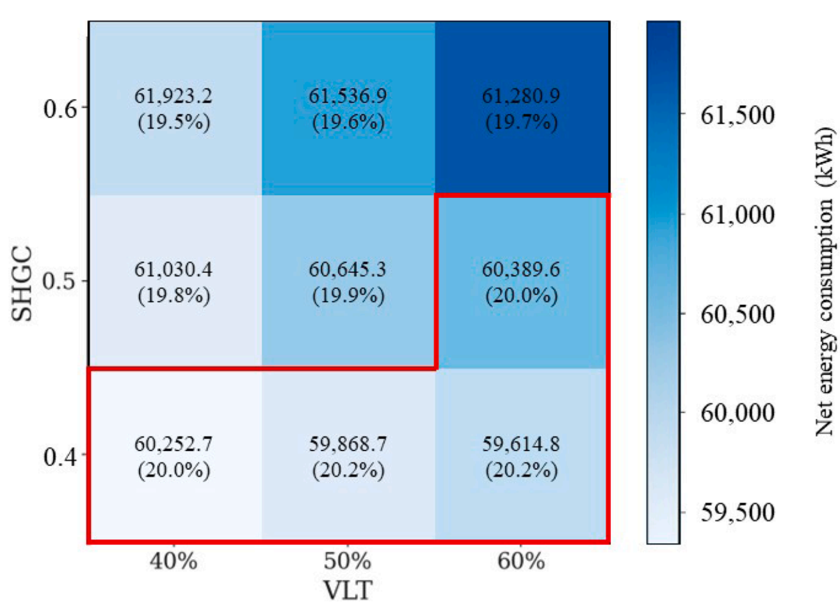

Fig. 13. Net energy consumption and ESSR of HSC_W with different VLT–SHGC combinations.

performance combinations. For each case, the annual energy consumption and PV generation were calculated, and the ESSR was derived to assess the feasibility of meeting the ZEB Grade 5 criteria. The main conclusions of this study are as follows:

(1) Evaluation of the indoor environment performance using mock-up experiments revealed distinct differences in the luminous and thermal characteristics of HSC_W and the Low-e windows. Due to its lower VLT (39.3 % for HSC_W and 66.1 % for Low-e windows), HSC_W had a markedly lower indoor illuminance, with the maximum illuminance under HSC_W reaching only ~48.5 % of that under Low-e windows. Similarly, the lower SHGC for HSC_W compared with the Low-e windows (0.383 and 0.590, respectively) limited the rise in the indoor air temperature by reducing the solar heat gain. PV generation was highly correlated with vertical plane solar radiation, but the practical performance of the solar cells was lower than the nominal efficiency due to seasonal variability and structural constraints.

(2) Building energy performance analysis was conducted through computer simulations. The EUI of the simulated building was 71.7 $kWh/m^2 \cdot yr$, which fell within the IQR range of 61 building samples with similar characteristics, confirming the reliability of the model. PV generation was also validated in a comparison with mock-up experimental data, with the NMBE of 3.5 % satisfying ASHRAE Guideline 14 standards. Overall, HSC_W reduced the total energy consumption by 1.3 % by decreasing the cooling energy consumption by 14.6 %, despite an increase of 9.5 % in heating energy and 6.0 % in lighting energy. This indicates that, in office buildings where cooling loads are higher, the solar radiation blocking performance of HSC_W effectively contributes to energy savings. In addition, through PV generation, 12,066.2 kWh of electricity was produced annually, reducing energy consumption by approximately 21.1 % compared with Low-e windows and achieving a high energy offset rate of up to 81.6 % during the spring and fall seasons.

(3) When varying the thermo-optical properties of HSC_W, differences of up to 2.73 % in the energy consumption were observed depending on the combination of the VLT and SHGC. Increasing the VLT reduced the lighting energy consumption, whereas decreasing the SHGC lowered the cooling energy consumption. The optimal combination was found to be Case 7 (VLT: 60 %; SHGC: 0.4), which achieved an additional 2.27 % reduction in energy consumption relative to Low-e windows by striking a balance between maximizing natural lighting and minimizing the cooling load. In the assessment of ZEB Grade 5 feasibility, four of the nine VLT–SHGC combinations achieved an ESSR of 20 % or higher, satisfying current mandatory ZEB standards. This suggests that, by improving its thermo-optical properties, HSC_W can simultaneously achieve energy production and energy savings while potentially meeting mandatory ZEB policies.

In conclusion, the HSC_W system exhibits great promise as a window-integrated BIPV technology capable of simultaneously providing PV power generation and visible light transmittance, thus reducing the energy consumption of buildings. However, despite the horizontal arrangement of PV cells, which was designed to ensure outward visibility and admit daylight, the daylighting analysis indicated that the indoor illuminance did not meet the recommended threshold. In addition, integrating PV cells into window systems may lead to practical visual limitations, such as partial obstruction of outward views and irregular indoor shadow patterns, which should be taken into account when assessing user comfort and real-world applicability. Because the system influences both the indoor luminous and thermal environments, careful evaluation is required when applying it to buildings with varying functional and spatial characteristics. The HSC_W system is currently an early-stage technology, with the long-term objective of scaling up to full-size window applications. Achieving this goal requires further research to address technical issues such as changes in optical and thermal performance during large-area scaling, module stability, and structural reliability. Moreover, because this study focused on a specific building type and climate, additional research is needed to assess the applicability of the proposed design under various environmental conditions.

Accordingly, future research should evaluate the performance of HSC_W in residential, office, and educational facilities over a range of climate conditions to develop practical design guidelines. Design alternatives such as optimized PV cell spacing, semi-transparent PV integration, and improved optical configurations should also be explored to enhance daylighting performance and visual comfort while ensuring architectural compatibility. Furthermore, economic assessments, including system costs, energy savings, life-cycle costs, and payback period analysis, will be conducted to further clarify the practical feasibility and market potential of the HSC_W system. Overall, this study experimentally validated the power generation, thermal performance, and energy self-sufficiency contribution of the HSC_W system, demonstrating its potential as an energy-active building envelope. By providing full-scale experimental data and an integrated evaluation framework, this study offers academic, technological, and societal contributions to the advancement of next-generation window-integrated BIPV systems.

Declaration of generative AI and AI-assisted technologies in the writing process

During the preparation of this work, the authors used OpenAI's ChatGPT in order to improve its readability and language. After using this tool, the authors carefully reviewed and edited the content as needed and take full responsibility for the content of the publication.

CRediT authorship contribution statement

A Young Kim: Writing – review & editing, Writing – original draft, Validation, Software, Methodology. **Bo Rang Park:** Visualization, Methodology. **Yong Gi Jung:** Investigation, Formal analysis. **Sang Hun Yeon:** Investigation. **Yongseok Jun:** Resources, Data curation, Conceptualization. **Jin Woo Moon:** Supervision, Project administration, Funding acquisition, Conceptualization.

Declaration of competing interest

The authors declare that they have no known competing financial interests or personal relationships that could have appeared to influence the work reported in this paper.

Acknowledgements

This work was supported by the National Research Foundation of Korea (NRF) grant funded by the Korea government (MSIT) (No. RS-2023–00217322) and a Chung-Ang University Graduate Research Scholarship in 2024.

Data availability

The authors do not have permission to share data.

References

[1] IEA, IEA World Energy Statistics and Balances, International Energy Agency (IEA), 2023.

[2] I. Hamilton, O. Rapf, D.J. Kockat, D.S. Zuhaib, T. Abergel, M. Oppermann, Global Status Report For Buildings and Construction, United Nations Environmental Programme: Nairobi, Kenya, 2020.

[3] ESG Today, EU Adopts Rules Requiring all New Buildings to Be Zero Emissions By 2030, 2024. https://www.esgtoday.com/eu-adopts-law-requiring-all-new-buildings-to-be-zero-emissions-by-2030/. accessed 5 June 2025.

[4] The White House, Fact sheet: Inflation Reduction Act, 2022. https://www.whitehouse.gov/briefing-room/statements-releases/2022/08/16/fact-sheet-inflation-reduction-act/. accessed 5 June 2025.
[5] Ministry of the Environment Japan, ZEH/ZEB policy (in Japanese). https://www.env.go.jp/policy/zeh-zeb/, 2023 (accessed 5 June 2025).
[6] China Academy of Building Research, Introduction to China's green Building Certification, 2023. https://www.cabr.com.cn/en/greenbuilding/. accessed 5 June 2025.
[7] N.-B. Park, Korean 2050 carbon neutrality scenarios: a comparative review and implications, Korean Clim. Change Res. 13 (2022) 689–704, https://doi.org/10.15531/KSCCR.2022.13.5.689.
[8] Statistics Korea, A Basic Study on Developing SDGs Indicators Related to 2050 Carbon Neutrality, Statistics Korea, 2022. https://mods.go.kr/board.es?mid=a90101010200&bid=11887&act=view&list_no=424832. accessed 5 June 2025.
[9] Korea Energy Agency, Zero Energy Building Information Portal, 2025. https://min24.energy.or.kr/nzeb/BC/BC03/BC03_05_002.do. accessed 3 September 2025.
[10] S.H. Lee, J. Kim, Decarbonization scenarios for residential building sector in South Korea: accelerating retrofit and mandating zero-energy buildings, Phase Transitions 95 (2022) 1–14, https://doi.org/10.1080/14786451.2022.2121398.
[11] Korea New and Renewable Energy Center, Results of 2023 Renewable Energy Supply Statistics, 2024. https://www.knrec.or.kr/biz/pds/statistic/view.do?no=390. accessed 3 February 2025.
[12] N. Martín Chivelet, C. Kapsis, F. Frontini (Eds.), Building-Integrated Photovoltaics: A Technical Guidebook,, 1st ed, CRC Press, London, 2025, https://doi.org/10.1201/9781003432241.
[13] B.R. Park, Y.J. Choi, A.Y. Kim, J.W. Moon, Climate-zone-dependent applicability of semi-transparent cadmium-telluride-type solar cells as a building material with display characteristics, Energy Build. 287 (2023) 112977, https://doi.org/10.1016/j.enbuild.2023.112977.
[14] J. Ding, S. Chai, T. Xu, Building-integrated photovoltaics (BIPV) in building performance research: a systematic literature review, Archit. Sci. Rev. 68 (2025) 1–22. https://archscience.org/wp-content/uploads/2025/03/Building-integrated-photovoltaics-BIPV-in-building-performance-research-a-systematic-literature-review-.pdf.
[15] V. Ratia, Temperature Effects and Degradation of Building Integrated Photovoltaics, 2025. https://www.utupub.fi/bitstream/10024/181936/1/Valtteri_Ratia_thesis.pdf.
[16] International Energy Agency, Trends in PV Applications 2025: Report IEA-PVPS T1-44:2025, IEA, Paris, 2025. https://iea-pvps.org/trends_reports/trends-2025/.
[17] M. Chen, W. Zhang, L. Xie, Z. Ni, Q. Wei, W. Wang, H. Tian, Experimental and numerical evaluation of the crystalline silicon PV window under the climatic conditions in southwest China, Energy 183 (2019) 584–598, https://doi.org/10.1016/j.energy.2019.06.176.
[18] A. Mesloub, G.A. Albaqawy, M.Z. Kandar, The optimum performance of building integrated photovoltaic (BIPV) windows under a semi-arid climate in Algerian office buildings, Sustainability. 12 (2020) 1654, https://doi.org/10.3390/su12041654.
[19] A. Ghosh, N. Sarmah, S. Sundaram, T.K. Mallick, Numerical studies of thermal comfort for semi-transparent building integrated photovoltaic (BIPV)-vacuum glazing system, Sol. Energy 190 (2019) 608–616, https://doi.org/10.1016/j.solener.2019.08.073.
[20] E. Cuce, S. Riffat, TiO_2 nano-coated thin film PV glazing with superior thermal and daylighting performance: experimental and numerical analysis, Int. J. Low-Carbon Technol. 17 (2022) 985–996, https://doi.org/10.1093/ijlct/ctab080.
[21] J. Xue, S. Wang, S. Wang, Review of different types of photovoltaic windows: performance, technology and integration, Renew. Sustain. Energy Rev. 158 (2022) 112164, https://doi.org/10.1016/j.rser.2022.112164.
[22] J. Kim, H. Lee, M. Choi, D. Kim, J. Yoon, Power performance assessment of PV blinds system considering self-shading effects, Sol. Energy 262 (2023) 111834, https://doi.org/10.1016/j.solener.2023.111834.
[23] Coherent Market Insights, Building Integrated Photovoltaics Market Size & Trends, 2025, p. 2032. https://www.coherentmarketinsights.com/industry-reports/building-integrated-photovoltaics-market. accessed Nov. 19, 2025.
[24] Y.T. Chae, J. Kim, H. Park, B. Shin, Building energy performance evaluation of building integrated photovoltaic (BIPV) window with semi-transparent solar cells, Build. Environ. 129 (2018) 217–227, https://doi.org/10.1016/j.buildenv.2017.12.027.
[25] Y. Feng, K. Fong, L. Wang, Z. Lin, Influence of building-integrated semi-transparent photovoltaics on energy performance of high-rise buildings, Appl. Energy 291 (2021) 116858, https://doi.org/10.1016/j.apenergy.2021.116858.
[26] X. Liang, Q. Pang, I.R. Kochetkov, M. Safont Sempere, H. Huang, X. Sun, L.F. Nazar, A facile surface chemistry route to a stabilized lithium metal anode, Nat. Energy 2 (2017) 17119, https://doi.org/10.1038/nenergy.2017.119.
[27] N. Skandalos, D. Karamanis, Investigation of thermal performance of semi-transparent PV technologies, Energy Build. 124 (2016) 19–34, https://doi.org/10.1016/j.enbuild.2016.04.060.
[28] Y. Peng, L. Lu, H. Yang, Review on life cycle assessment of energy payback and greenhouse gas emission of solar photovoltaic systems, Appl. Energy 183 (2016) 781–802, https://doi.org/10.1016/j.apenergy.2016.09.072.
[29] S.L. Do, M. Shin, J.C. Baltazar, J. Kim, Energy benefits from semi-transparent BIPV window and daylight-dimming systems for IECC code-compliance residential buildings in hot and humid climates, Sol. Energy 155 (2017) 291–303.
[30] L. Chen, Y. Li, W. Zhou, L. Wang, Z. Lin, Modelling the effect of BIPV window in the built environment, Energy Build. 261 (2022) 112496, https://doi.org/10.1016/j.buildenv.2021.108605.
[31] B. Joseph, T. Pogrebnaya, T. Kichonge, Semitransparent building-integrated photovoltaic: review on energy performance, challenges, and future potential, Int. J. Photoenergy 2019 (2019) 1–15, https://doi.org/10.1155/2019/5214150.
[32] X. Li, M. Wang, A review of complex window-glazing systems for building integration: thermal, optical and electrical properties, Build. Serv. Eng. Res. Technol. 46 (2025) 130–157, https://doi.org/10.1177/17442591241269182.
[33] C.J. Traverse, R. Pandey, M.C. Barr, R.R. Lunt, Emergence of highly transparent photovoltaics for distributed applications, Nat. Energy 2 (2017) 849–860, https://doi.org/10.1038/s41560-017-0016-9.
[34] T. Hoang, J.D. Lee, A. Sandanayaka, E. Matsubara, K. Okada, M. Sugiyama, C. Goushi, R. Zeika, S. Adachi, C. Adachi, D.Y. Kim, Highly efficient, transparent organic solar cells with enhanced stability for building-integrated photovoltaics, Build. Environ. 210 (2022) 108615, https://doi.org/10.1016/j.buildenv.2021.108615.
[35] X. Meng, Z. Wang, C. Li, Review on mechanical behavior of solar cells for building integrated photovoltaics (BIPV), Sustain. Technol. 1 (2021) 000009. http://www.sustain-dpl.com/UploadFile/article/202210011130541341.pdf.
[36] Z.R.K. Abojela, F. Sun, D. Dai, Current prospects of building-integrated solar PV systems: a review, Front. Energy Res. 11 (2023) 1164494, https://doi.org/10.3389/fenrg.2023.1164494.
[37] A. Machín, J.M. Asensio, R. Prieto, Advancements in photovoltaic cell materials: silicon, organic, and perovskite solar cells, Materials 17 (2024) 1165, https://doi.org/10.3390/ma17051165.
[38] Ministry of Land, Infrastructure and Transport, Building Energy Saving Design Standards, MLIT Notice No. 2023-104, 2023.
[39] International Organization for Standardization, ISO 9060:2018, Solar energy – Specification and Classification of Instruments for Measuring Hemispherical Solar and Direct Solar Radiation, ISO, Geneva, 2018.
[40] DesignBuilder Software Ltd, DesignBuilder v7.0.2.003 [software], DesignBuilder Software Ltd, 2023. https://designbuilder.co.uk/. accessed 3 September 2025.
[41] DesignBuilder Software Ltd, DesignBuilder – EnergyPlus Background Information, 2025. https://designbuilder.co.uk/helpv7.0/Content/_EnergyPlus_background_information.htm. accessed 17 January 2025.
[42] V. Garg, J. Mathur, A. Bhatia, Building Energy Simulation: A Workbook Using DesignBuilder™, CRC Press, Boca Raton, 2020.
[43] M. Baharvand, M. Hamdan, M. Abdul, DesignBuilder verification and validation for indoor natural ventilation, J. Basic Appl. Sci. Res. 3 (2013) 8.
[44] G. Elshafei, A. Negm, M. Bady, M. Suzuki, M.G. Ibrahim, Numerical and experimental investigations of the impacts of window parameters on indoor natural ventilation in a residential building, Energy Build. 141 (2017) 321–332, https://doi.org/10.1016/j.enbuild.2017.02.044.
[45] A. Fathalian, H. Kargarsharifabad, Actual validation of energy simulation and investigation of energy management strategies (Case study: an office building in Semnan, Iran), Case Stud. Therm. Eng. 12 (2018) 510–516, https://doi.org/10.1016/j.csite.2018.04.022.
[46] J.H. Kim, J.H. Lee, S.J. Kim, Comparative analysis of building energy performance using ECO2 and DesignBuilder for small green remodeling public buildings, J. Korean Sol. Energy Soc. 42 (2022) 91–100, https://doi.org/10.7836/kses.2022.42.3.91.
[47] Korea Energy Agency, Zero Energy Building Certification Technical Elements Reference Guide, Ulsan, 2020.
[48] J.H. Kim, J.E. Sung, H.K. Kim, D.J. Park, S.S. Kim, Improvement of office building energy performance due to strengthening of building energy saving design standards, J. Korean Inst. Arch. Sustain. Facility Eng. 14 (2020) 101–111, https://doi.org/10.22696/jkiaebs.20200010.
[49] DesignBuilder, Lighting control. https://designbuilder.co.uk, (accessed 25 September 2025).
[50] S. Kim, S. Jung, J.C. Park, Energy-saving effect analysis of dimming control algorithms via building simulation, J. Archit. Inst. Korea 32 (2016) 101–112, https://doi.org/10.5659/JAIK.2016.32.2.101.
[51] Climate.OneBuilding.org, Global Weather Data Files for Building Simulation, 2025. https://climate.onebuilding.org/. accessed 19 December 2024.
[52] Lawrence Berkeley National Laboratory, Windows & Daylighting Research Group. https://windows.lbl.gov/, 2024 (accessed 17 November 2024).
[53] Lawrence Berkeley National Laboratory, WINDOW6 [software], LBNL, 2019.
[54] KCC, KCC Coated Glass Product Information, 2024. https://www.kccglass.co.kr/eng/main.do. accessed 20 September 2024.
[55] Architecture HUB Portal, Architecture HUB Architectural Services Industry Information System, 2024. https://www.hub.go.kr/portal/gis/bld/idx-bld-list.do. accessed 6 November 2024.
[56] e-Nara Indicators, Building Status – Statistics by Gross Floor area, usage, Region, 2024. https://www.index.go.kr/unity/potal/main/EachDtlPageDetail.do?idx_cd=1226. accessed 6 November 2024.
[57] DesignBuilder Software Ltd, DesignBuilder Official Manual – Solar collector and PV Settings, 2025. https://designbuilder.co.uk/helpv7.0/Content/SolarCollectorDataConstructionTab.htm. accessed 7 July 2025.
[58] R. Coakley, P. Raftery, M. Keane, A review of methods to match building energy simulation models to measured data, Build. Environ. 84 (2015) 152–165, https://doi.org/10.1016/j.buildenv.2014.11.042.
[59] J. Sun, G. Augenbroe, Calibration of building energy simulation models: a review of uncertainty analysis and optimization methods, Build. Environ. 105 (2016) 273–287, https://doi.org/10.1016/j.buildenv.2016.05.032.
[60] J. Bermeo-Ayerbe, J. Ortiz, J.L. Salmerón, A critical review of building energy model calibration methods based on in-situ measurements, Build. Environ. 205 (2021) 108246, https://doi.org/10.1016/j.buildenv.2021.108246.

[61] U.S. Green Building Council, LEED v4.1 BD+C Reference Guide, U.S. Green Building Council, 2021.
[62] BRE, BREEAM International New Construction Technical Manual, BRE Global Ltd., 2022.
[63] Ministry of Environment, Ministry of Land, Infrastructure and Transport, G-SEED Certification Criteria, MOE Notice No. 2022-49, MLIT Notice No. 2022-35, 2022, 2022.
[64] Ministry of Employment and Labor, Rules on Occupational Safety and Health Standards, Article 8 (Illumination), MOEL Ordinance No. 163, 2023. https://hseworld.co.kr/52. accessed 8 July 2025.
[65] Ministry of Land, Infrastructure and Transport, Rules on Building Equipment Standards, MLIT Ordinance No. 642, 2022.
[66] C. Peng, J. Yang, The effect of photovoltaic panels on the rooftop temperature in the EnergyPlus simulation environment, Energy 104 (2016) 116–124, https://doi.org/10.1016/j.energy.2016.03.102.